

Preliminary Report

**DESIGN STUDY FOR A LOW ENRICHED
URANIUM (LEU) CORE FOR THE
HIGH FLUX ISOTOPE REACTOR (HFIR)**

**R. T. Primm III
R. J. Ellis
J. C. Gehin**

April 20, 2006

DOCUMENT AVAILABILITY

Reports produced after January 1, 1996, are generally available free via the U.S. Department of Energy (DOE) Information Bridge.

Web site <http://www.osti.gov/bridge>

Reports produced before January 1, 1996, may be purchased by members of the public from the following source.

National Technical Information Service
5285 Port Royal Road
Springfield, VA 22161
Telephone 703-605-6000 (1-800-553-6847)
TDD 703-487-4639
Fax 703-605-6900
E-mail info@ntis.fedworld.gov
Web site <http://www.ntis.gov/support/ordernowabout.htm>

Reports are available to DOE employees, DOE contractors, Energy Technology Data Exchange (ETDE) representatives, and International Nuclear Information System (INIS) representatives from the following source.

Office of Scientific and Technical Information
P.O. Box 62
Oak Ridge, TN 37831
Telephone 865-576-8401
Fax 865-576-5728
E-mail reports@osti.gov
Web site <http://www.osti.gov/contact.html>

This report was prepared as an account of work sponsored by an agency of the United States Government. Neither the United States government nor any agency thereof, nor any of their employees, makes any warranty, express or implied, or assumes any legal liability or responsibility for the accuracy, completeness, or usefulness of any information, apparatus, product, or process disclosed, or represents that its use would not infringe privately owned rights. Reference herein to any specific commercial product, process, or service by trade name, trademark, manufacturer, or otherwise, does not necessarily constitute or imply its endorsement, recommendation, or favoring by the United States Government or any agency thereof. The views and opinions of authors expressed herein do not necessarily state or reflect those of the United States Government or any agency thereof.

Preliminary Report

**DESIGN STUDY FOR A LOW ENRICHED URANIUM (LEU) CORE
FOR THE HIGH FLUX ISOTOPE REACTOR (HFIR)**

**R. T. Primm, III
R. J. Ellis
J. C. Gehin**

Date Published: April 20, 2006

Prepared by
OAK RIDGE NATIONAL LABORATORY
P.O. Box 2008
Oak Ridge, Tennessee 37831-6283
managed by
UT-Battelle, LLC
for the
U.S. DEPARTMENT OF ENERGY
under contract DE-AC05-00OR22725

CONTENTS

LIST OF FIGURES	v
LIST OF TABLES	vii
ABSTRACT	ix
1. INTRODUCTION	1
2. NEUTRONICS ANALYSIS	2
3. THERMAL HYDRAULIC ANALYSIS	17
4. PERFORMANCE INDICTORS	22
5. IMPLICATIONS FOR FUEL PLATE DESIGN AND FABRICATION	25
6. REFERENCES	26
APPENDIX: FUEL PARAMETER LIST	27

LIST OF FIGURES

2.1	Schematic of the IFE and OFE fuel plates.....	3
2.2	Comparison of k vs. time for the LEU and HEU cores (without control absorber insertion) as calculated with VENTURE	5
2.3	Simulated operating criticality by modeled control absorber movement	6
2.4	HEU case with control absorber insertion, at BOL	7
2.5	LEU case with fuel grading, with control absorber insertion, at BOL	7
2.6	HEU case with control absorber insertion, at EOL.....	8
2.7	LEU case with fuel grading, with control absorber insertion, at EOL.....	8
2.8	Representative axial neutron flux profiles in HFIR (this case is LEU, with no control absorber insertion, at BOL)	9
2.9	Power contours in the Inner HFIR fuel elements (LEU at left, HEU at right) at BOL.....	11
2.10	Power contours in the Outer HFIR fuel elements (LEU at left, HEU at right) at BOL.....	11
2.11	Sections of fuel elements visualized in succeeding graphs.....	12
2.12	Burn-up distribution in LEU core at EOL	13
2.13	Power distribution in HEU core at BOL and EOL	14
2.14	Power distribution in LEU core at BOL and EOL.....	15

LIST OF TABLES

1.1	Quantities to be computed in HFIR LEU study	1
2.1	HFIR fuel region homogenized average atom densities with LEU	3
2.2	Comparison of VENTURE and MCNP results for K_{eff} for BOL HFIR cores with no control absorber insertion	5
2.3	Comparison of relative changes in HFIR thermal neutron flux characteristics (mid-plane) between the HEU and LEU cores, using MCNP5 flux tallies	6
2.4	Comparison of fuel meat thicknesses for LEU and HEU fuel plates.....	13
2.5	Peak thermal neutron flux levels as predicted by VENTURE for HEU and LEU cases	16
2.6	Comparison of HFIR isotope content (kg) in LEU and HEU cores, at BOL and EOL	16
3.1	Flux peaking factors for fuel extending beyond normal axial boundaries of the fuel plate (flow entrance and exit)	17
3.2	Incipient boiling power ratios	18
3.3	LEU burn-up-dependent heat transfer data—incipient boiling criteria	19
3.4	Burn-up-dependent heat transfer data—incipient boiling criteria—for HEU fuel	20
3.5	LEU burn-up-dependent heat transfer data—incipient boiling criteria—with perfectly engineered elements and perfect reactor operation.....	21
3.6	Burn-up-dependent heat transfer data—incipient boiling criteria—with perfectly engineered elements and perfect reactor operation for HEU fuel.....	22
4.1	Reflector flux performance	23
4.2	Central target flux performance	24

ABSTRACT

Initial neutronics studies show that, for equivalent operating power (85 Megawatts –thermal), a low enriched uranium (LEU) fuel cycle based on uranium-10 weight percent molybdenum metal foil with radially, “continuously graded” fuel meat thickness results in a 10 percent reduction in peak thermal flux in the beryllium reflector of the High Flux Isotope Reactor (HFIR) as compared to the current high enriched uranium (HEU) cycle. The uranium-235 content of the LEU core is twice the amount of the HEU core when the length of the fuel cycle is kept the same for both fuels. However, due to higher local power densities that exist at the fuel edges in the LEU core relative to the HEU core, the LEU core considered in this study cannot be operated at the same power level as the current HEU core. The power-limiting impact of higher power peaking in the LEU core is a significant loss of margin to the steady-state incipient boiling limit. A 19 percent reduction in operating power would be required when fueling the HFIR with LEU. The consequence of these two factors, neutronics and thermal hydraulics, results in a 27 percent decrease (factors are multiplicative) in the peak thermal flux in the beryllium reflector of the HFIR for the LEU cycle as compared to the current HEU cycle. The minimum foil thickness of 5 mils is a constraint on the radial fuel grading profile and power peaking for the LEU core. There is no attempt at this time to address either axially-variable burnable poison loading or axial fuel grading to minimize the axial power peaking since such design options are outside the bases for the study as defined in the assumptions and criteria report. Implications of the preliminary results on the fuel plate design and fabrication are discussed.

Annual plutonium production from fueling HFIR with LEU is predicted to be two kilograms.

These studies are preliminary and several physics parameters have yet to be calculated. ORNL staff are continuing to search for engineering designs that minimize or eliminate the flux penalty.

1.0 INTRODUCTION

Design studies for a low enriched uranium (LEU) core for the High Flux Isotope Reactor (HFIR) are being conducted according to the plan documented in Ref. 1. A summary of the studies to be conducted during fiscal year 2006 is presented in Table 1.1 (from Ref. 1). Results are available for only some of the quantities listed in Table 1.1, and none of the calculations have been reviewed.

Neutronics and thermal hydraulics work performed to date is being reported. Performance indicators for an LEU fuelled core relative to the current, high enriched uranium (HEU) core are presented. Summary documentation for the current, HEU cycle was requested by the RERTR program and is included as an appendix.

Table 1.1 Quantities to be computed in HFIR LEU study

Safety parameters

- Doppler reactivity coefficient
- Void reactivity coefficient
- Control element differential reactivity worth
- Safety rod reactivity worth (with one stuck element)
- Central void maximum reactivity worth
- Fuel element criticality (elements together and separate in light water and reflected by concrete)
- Fuel element decay heat

Performance parameters

- Cycle length
- Power distribution
- Neutron flux in the central target region
- Peak unperturbed thermal flux in the reflector
- Thermal flux at the HB-2 beam tube
- Thermal flux at the NAA irradiation location
- Cold source flux

Other parameters (safeguards and environmental)

- Plutonium content in spent fuel elements
 - Fuel element dose rates
 - Fuel element isotopic compositions
-

2.0 NEUTRONICS ANALYSES

The process for choosing a plausible LEU fueling design for HFIR, using uranium-10 weight percent molybdenum (U-10Mo) alloy involved an iterative process initially assessing the beginning-of-life (BOL) reactivity of the HFIR reactor core. All of the studies reported in this document assume that the fuel is a U-10Mo alloy foil without a diffusion barrier between the fuel meat and clad. Table 2.1 presents nominal atom densities for the LEU fuel in the HFIR core inner and outer fuel elements (IFE and OFE). MCNP5 was used with a detailed model of HFIR (cycle 400) adapted for U-10Mo fuel. The initial trial involved testing the U-10Mo core at BOL with the same amount of uranium-235 (^{235}U) as the standard HEU core. The k -effective (k_{eff}) of this arrangement was seen to be clearly subcritical, because of the effects of the large concentration of uranium-238 (^{238}U) and to a lesser extent, the concentration of natural Mo. The MCNP results for this case, which is the nominal standard critical configuration case, were $k_{\text{eff}}=0.9251\pm 0.0012$. The loading of ^{235}U was increased to increase the core reactivity and value of k_{eff} . Concurrently, corresponding VENTURE models were run to assess the calculated k_{eff} at the target 26 day end-of-life (EOL). Table 2.2 shows the MCNP k_{eff} determination results for the LEU core compared to the HEU core. Further MCNP analyses have indicated that the reactivity effect of the natural elemental Mo in the LEU core is a reactivity load of $-1.98\%\Delta k$.

The postulated U-10Mo loading of the HFIR core has 2.05 times the amount of ^{235}U as the standard HEU core in Cycle 400. The density of the monolithic U-10Mo material is 17.02 g/cm^3 . For the LEU design with 2.05 times the ^{235}U as in Cycle 400, the thickness of the fuel meat in the plates ranges from 0.0125 cm (5 mil) to 0.0305 cm (12 mil) for IFE plates, and 0.0165 cm (6.5 mil) to 0.0448 cm (17.6 mil) for the OFE. The fuel grading profile is the same as the current (Fig.1) HEU fueled core plates. The boron-10 (^{10}B) loading of the fuel plates in IFE is 2.8 g, distributed in the fuel meat filler region of the plates. It should be noted that the thickness of the U-10Mo fuel meat is much thinner than the fueled portion of the HEU fuel plates, by almost a factor of three. Because of this, the region of the U-10Mo fuel plates that is filled with the ^{10}B and the nearly pure aluminum alloy (Al-1100) filler mixture is almost a constant thickness thereby lacking the relatively large ratio of Al/ ^{10}B filler to uranium at the inner and outer edges of the IFE fuel element as seen in Fig. 2.1 for the HEU fuel. Consequently, the suppression of fission power generation at the inner and outer edges of the IFE fuel plates will not be as effective in the LEU case as in the HEU case.

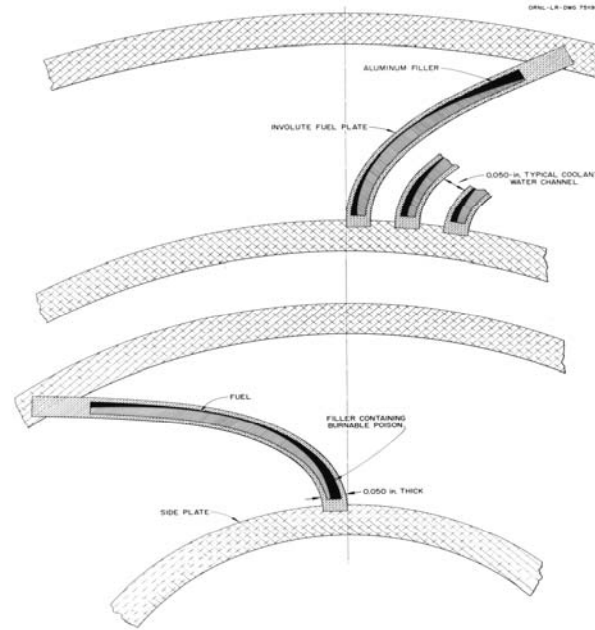


Fig. 2.1. Schematic of the IFE and OFE fuel plates.

The mass of ^{235}U per IFE plate is 37.975 g and for the OFE plates, 31.265 g. The total mass of ^{235}U in the LEU core is 19.358 kg, with 14.013 kg in the IFE and 5.346 kg in the OFE. The total mass of U-10Mo in the core is 108.913 kg. Table 2.1 lists the atom densities for the constituent isotopes (except for Al and minor constituent isotopes such as silicon) in the fuel meat and cladding, averaged or homogenized over the IFE and OFE active regions. The atom densities for the appropriate isotopes in the fuel plate alone are a factor of 2 larger than those listed in Table 2.1. The isotopes in the fuel meat portion of the fuel plate have actual atom density concentrations 3.30 times greater than the tabulated data (Table 2.1).

Table 2.1. HFIR fuel region homogenized average atom densities with LEU

Isotope/ID	IFE (atoms/barn-cm)	OFE (atoms/barn-cm)
B-10 (5010)	9.73032E-06	-
B-11 (5011)	3.94078E-05	-
Mo (42000)	1.09760E-03	1.46619E-03
U-234 (92234)	7.93670E-06	1.06019E-05
U-235 (92235)	7.96357E-04	1.06378E-03
U-236 (92236)	3.64770E-06	4.87264E-06
U-238 (92238)	3.18354E-03	4.25261E-03

The reference HEU core contains 9.4 kg of U-235. The LEU core design studied initially contained 19.36 kg of U-235, and 108.913 kg of U-10Mo in the core. The first graded LEU core design contains 19.264 kg of U-235, and 108.373 kg of U-10Mo.

Fig. 2.2 presents the results from VENTURE calculations for the k_{eff} behavior of the LEU core fuel designs compared to the reference HEU case. The presented cases are all without control absorber insertion to illustrate the excess reactivity behavior of the various cores. Both the HEU and LEU cores in HFIR show the expected significant drop in available core reactivity during the first day of operation due to the build-in of the fission product poison ^{135}Xe . As seen in the LEU cases, there is an

expected reactivity increase (Pu bump) at 1-2 days into the cycle due to plutonium-239 (^{239}Pu) build-in from the high concentration of ^{238}U . The reactivity of the LEU cores at 26 d is seen to be slightly greater than the reference HEU core case. This implies that the LEU core lifetime will meet the HEU length of lifetime criterion.

Table 2.2 presents the MCNP5 k_{eff} results for the HEU and initial LEU HFIR core at BOL without control absorber insertion and without xenon-135 (^{135}Xe), with temperature conditions as discussed in ORNL/TM-2004/251, in the MCNP documentation of HFIR Cycle 400. The HEU core is seen to have a considerably larger initial reactivity (that is, higher value of k_{eff}) than the LEU core.

Fig. 2.3 presents the critical k_{eff} behavior during the controlled HFIR operation in the 26 d simulated fuel cycles. The criticality profile is a function of the control absorber movements simulated in the VENTURE cases; the control element positioning as a function of days of full power operation is kept the same for the HEU and the LEU cases to facilitate comparison.

Table 2.3 is a comparison of HEU and LEU thermal neutron flux levels as calculated by MCNP5 tallies. The two core energy tallies for the two independent HFIR calculations were also gathered, and these are normalized to 85 MW to allow for the correct determination of the relative flux changes in the LEU core compared to the HEU core. As seen, the Flux Trap Target (FTT) peak thermal flux remains approximately the same, while the peak thermal neutron flux level in the Be reflector drops by approximately 9 percent in the LEU core compared to the HEU core. This will be discussed below with regards to similar VENTURE thermal neutron flux determinations.

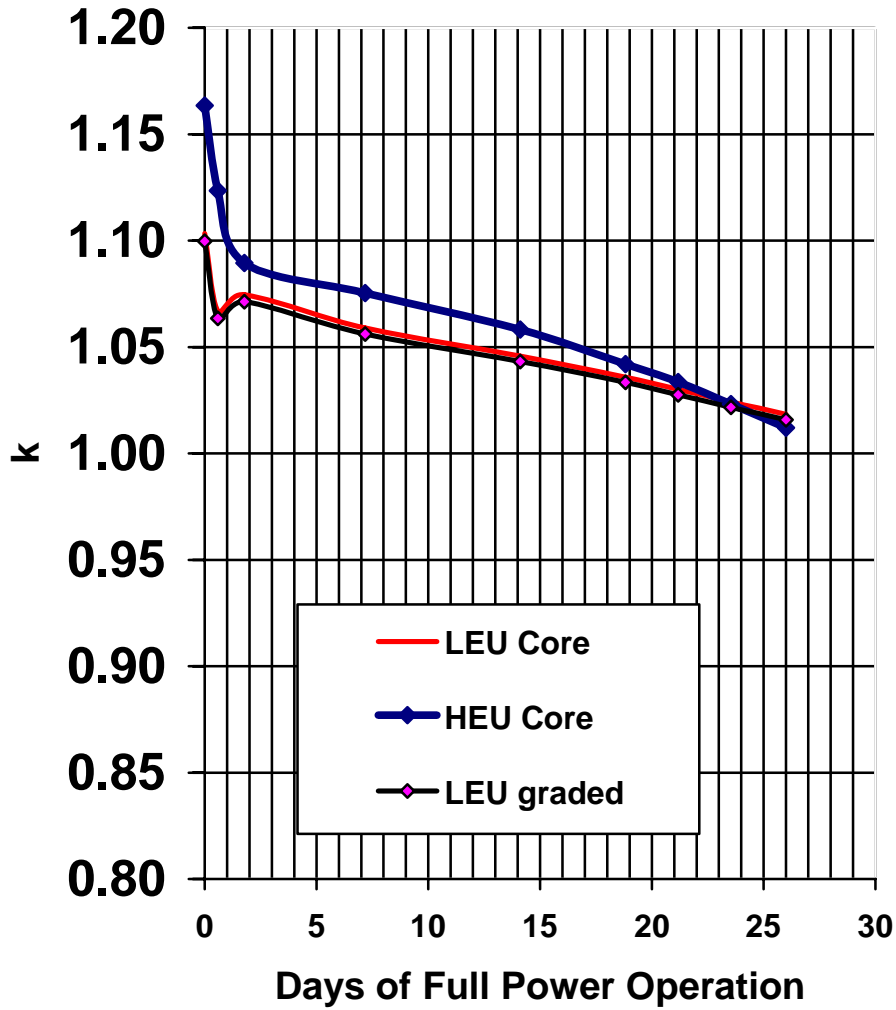


Fig. 2.2. Comparison of k vs. time for the LEU and HEU cores (without control absorber insertion) as calculated with VENTURE.

Table 2.2. Comparison of VENTURE and MCNP results for k_{eff} for BOL HFIR cores with no control absorber insertion

	LEU	HEU
MCNP	1.08682±0.00025	1.13574±0.00025
VENTURE	1.09972	1.16348

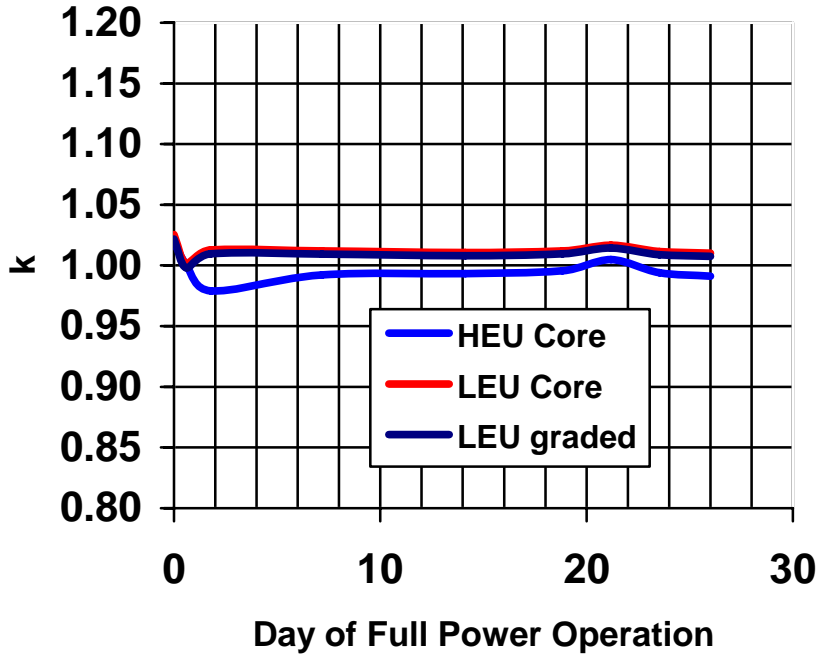


Fig. 2.3. Simulated operating criticality by modeled control absorber movement.

Table 2.3. Comparison of relative changes in HFIR thermal neutron flux characteristics (mid-plane) between the HEU and LEU cores, using MCNP5 flux tallies

New	LEU		HEU		HEU/LEU Ratio (Normalized by power)
	Tally	Relative Error	Tally	Relative Error	
FTT	0.000283390	.0164	0.000301793	.0159	1.016±0.032
Core Power	80.3808	.0003	84.2330	.0004	
Reflector	3.44207	.0008	3.95411	.0008	1.096±0.003

Figs. 2.4 to 2.8 present representative neutron flux distributions in the various HEU and LEU core simulations. The neutron flux traces are at mid-plane and the 20-energy-group neutron flux results from the VENTURE cases are collapsed to four convenient energy groups, with group 1 being fast, and group 4 being the thermal neutron flux. Fig. 2.8 is a representative plot of HFIR axial neutron flux distributions presented to illustrate the axial neutron flux profiles. All the radial plots (at mid-plane) show the thermal neutron flux depression at the location of the IFE and OFE fuel element regions. The thermal neutron flux depression is seen to be greater in the LEU cases, as expected by virtue of the greater ²³⁵U concentration. Also, the thermal neutron flux peaking in the FTT region is evident. The thermal neutron flux is seen to drop off quickly in the water region surrounding the reflector. Comparisons can be made to the similar distributions in the HEU and LEU cases.

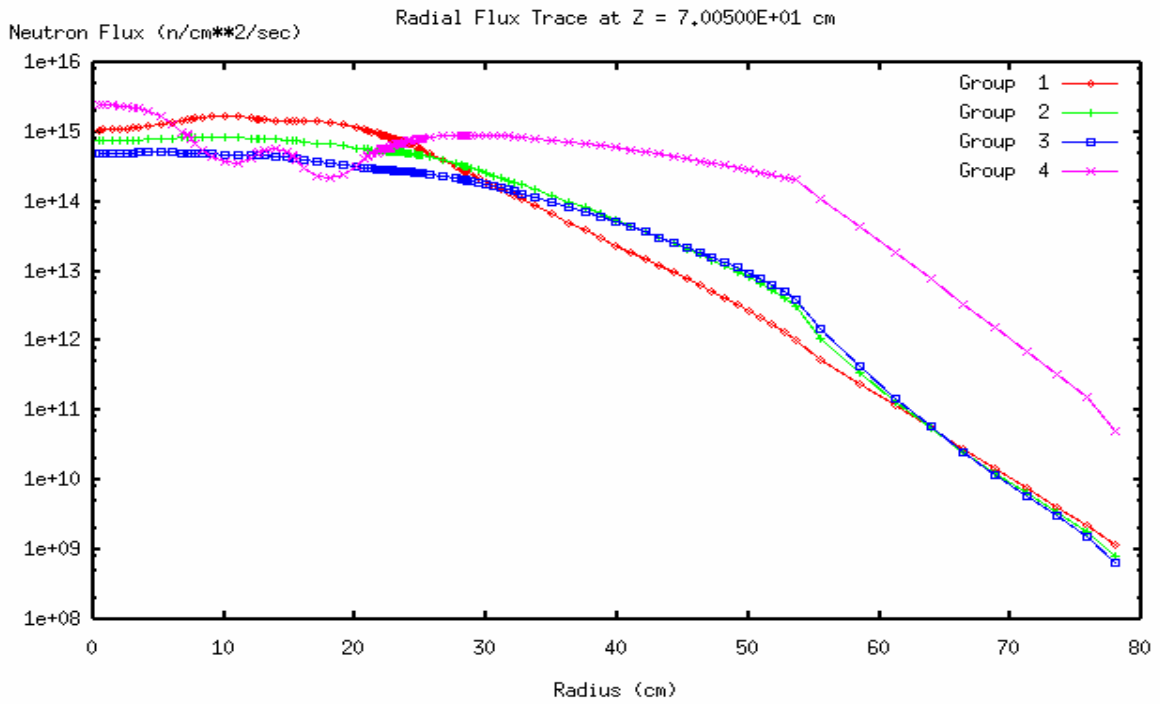


Fig. 2.4. HEU case with control absorber insertion, at BOL.

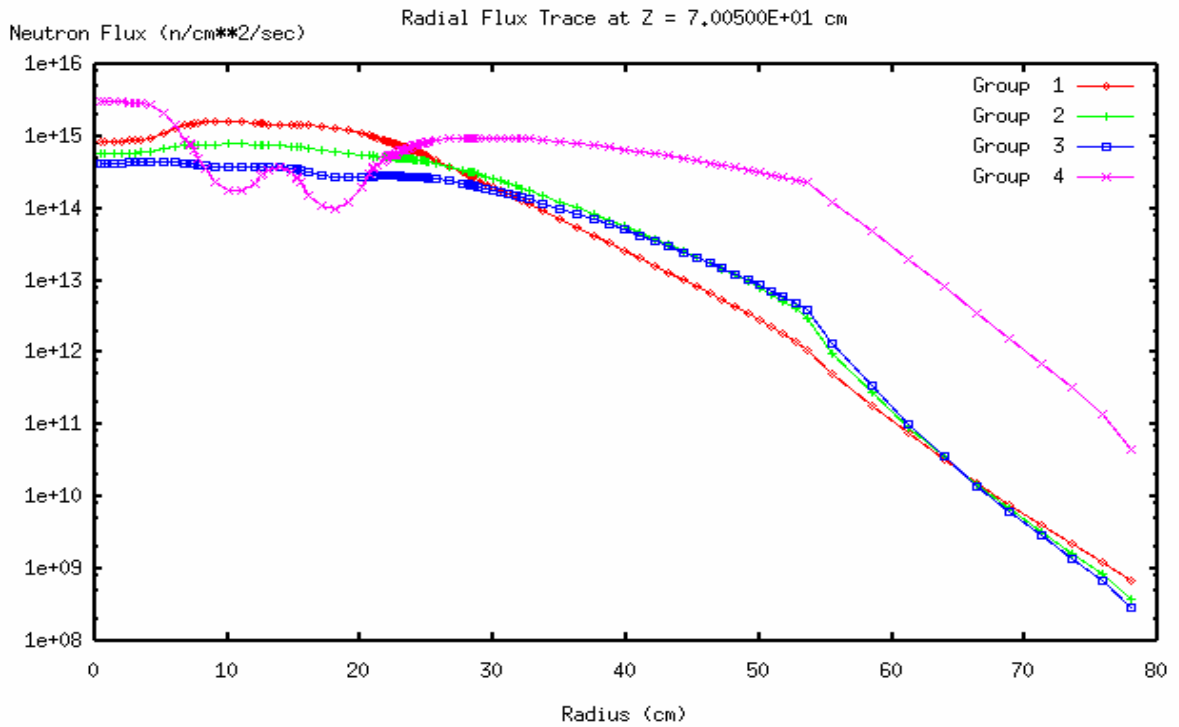


Fig. 2.5. LEU case with fuel grading, with control insertion, at BOL.

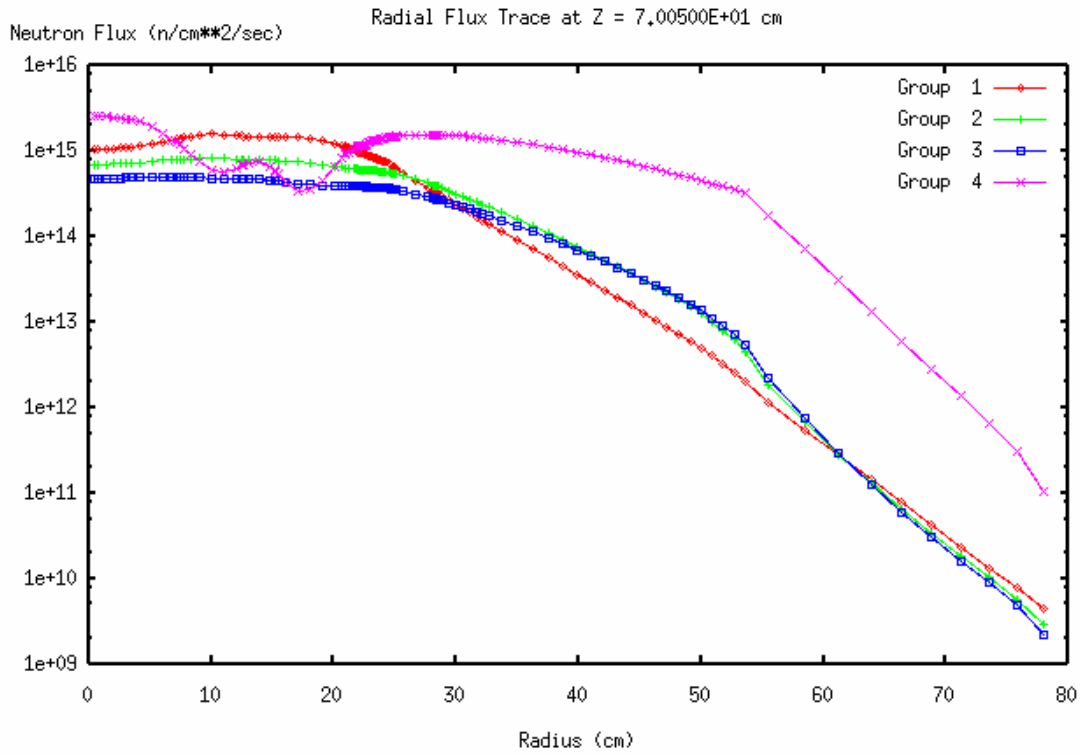


Fig. 2.6. HEU case with control absorber insertion, at EOL.

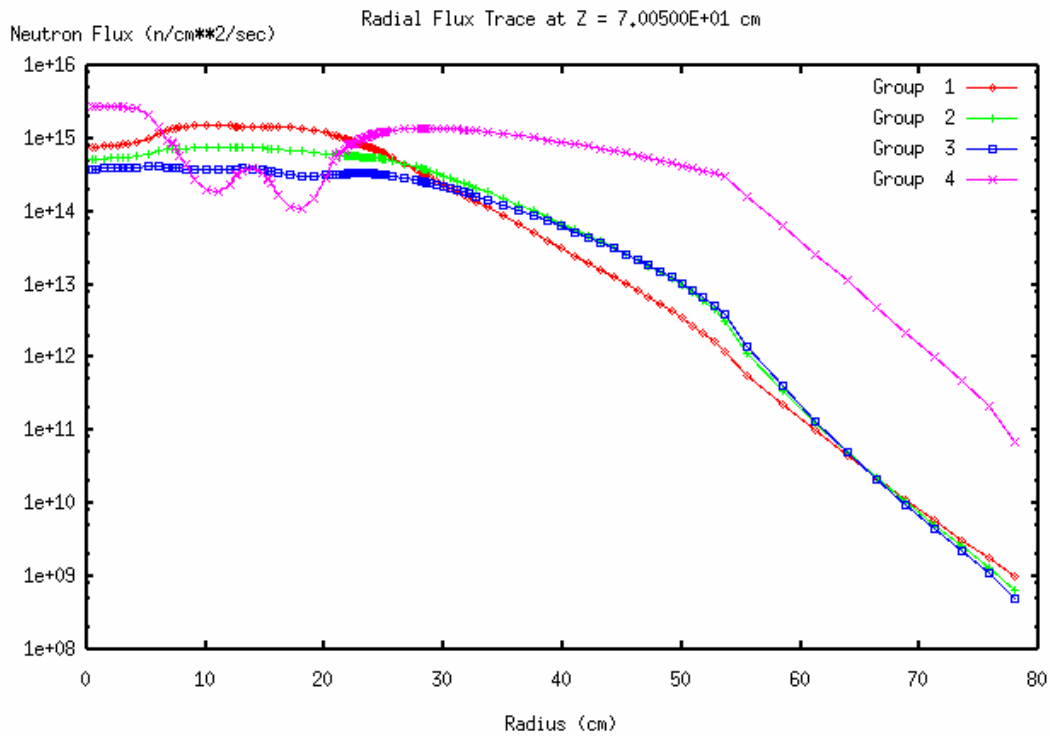


Fig. 2.7. LEU case with fuel grading, with control insertion, at EOL.

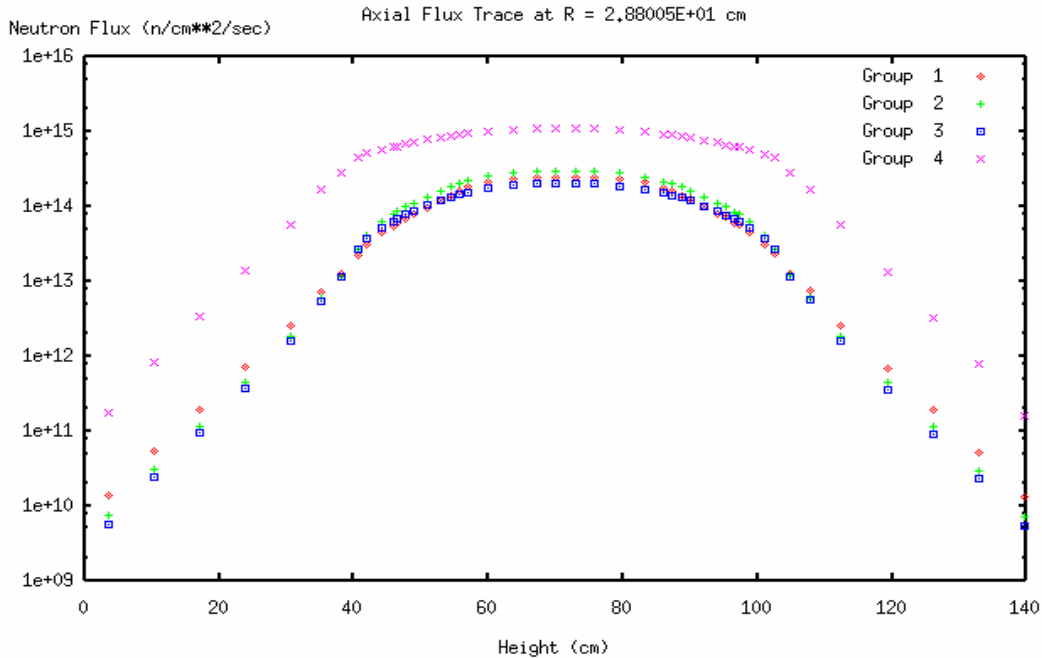


Fig. 2.8. Representative axial neutron flux profiles in HFIR (this case is LEU, with no control absorber insertion, at BOL).

Fig. 2.9 presents contour plots of the relative power distributions as calculated with VENTURE for the IFE in the graded LEU HFIR core and the current HEU core. These plots are at BOL. By comparison, Fig. 2.10 below presents the analogous OFE relative power distribution contours for the LEU and HEU cores, as calculated with VENTURE.

Succeeding figures in this report display physics parameters (fluxes, power distributions, burn-up) as a function of position in the reactor core. Figure 2.11 is provided to orient the reader as to the perspective shown in the figures. Fig. 2.12 presents the fuel burn-up distribution at EOL in the LEU core. The burn-up is seen to peak in the IFE, which is subject to relatively high peak power densities. As noted on the figure, the maximum local end-of-life burn-up is 61 percent of the initial ^{235}U atoms. The maximum local burn-up in the current, HEU fuel is 72 percent, slightly higher than the LEU core. For both the LEU and the HEU cores, maximum local burn-up occurs at essentially the same location – the axial mid-plane and at the inner edge of the inner element.

Figures 2.13 and 2.14 are simply different representations of the results shown in Figs. 2.9 and 2.10. Figure 2.13 shows a comparison of beginning-of-life power distribution for the current, HEU core and the preliminary LEU core. The LEU core shows higher local power densities at the radial and axial edges of the fuel elements due to the higher volumetric ^{235}U loading of the LEU core at these locations. Figure 2.14 provides a comparison of end-of-life power distribution for the current HEU core and the preliminary LEU core. Even at end-of-life, the radial and axial edges of the fuel in the LEU core are more highly peaked than the HEU core. (Note that the relative power density scale for Fig. 2.13 differs from Fig. 2.14.)

Table 2.4 provides a comparison of the thicknesses of the fuel meat regions for the LEU plates and the current HEU plates. Minimum and maximum fuel meat thicknesses for the LEU fuel are considerably less than that for the HEU fuel. Note that the minimum allowable LEU foil thickness (5 mils) is a constraint for the inner element plate.

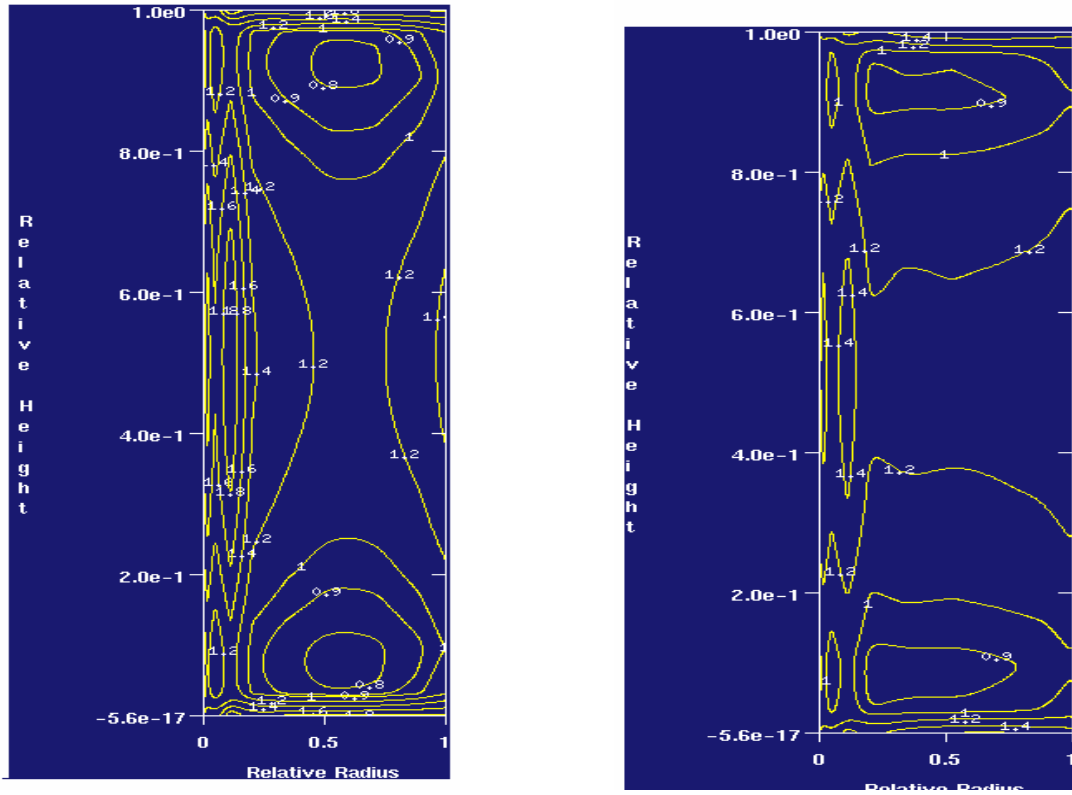


Fig. 2.9. Power contours in the Inner HFIR fuel elements (LEU at left, HEU at right) at BOL.

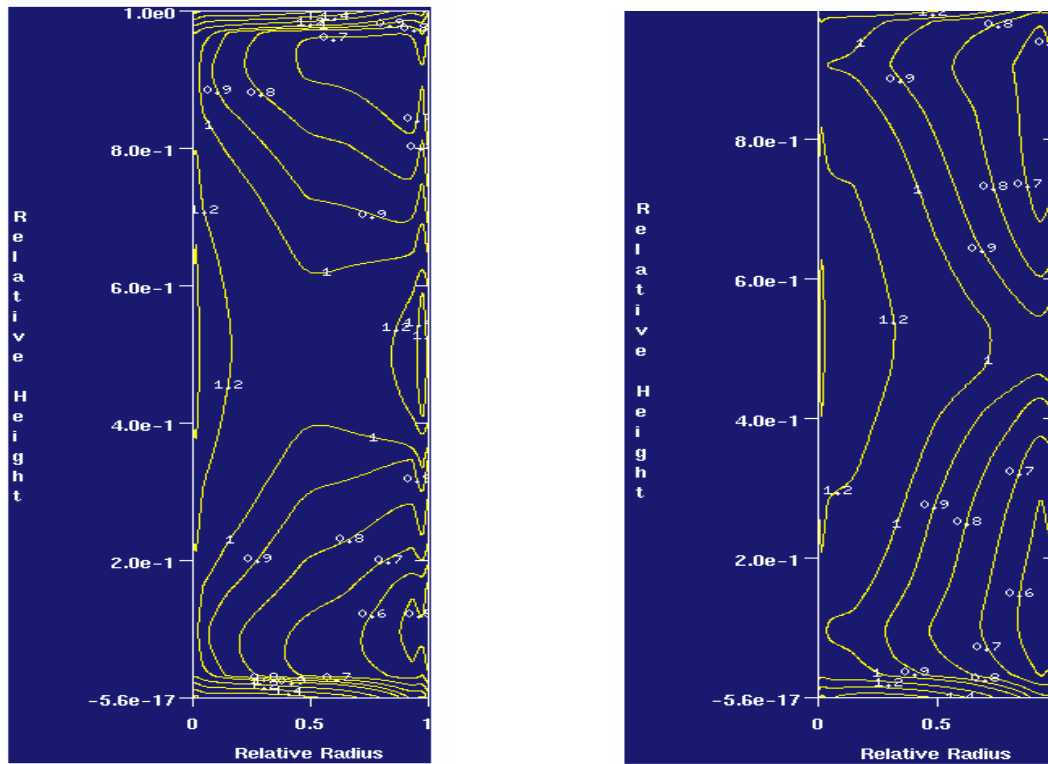
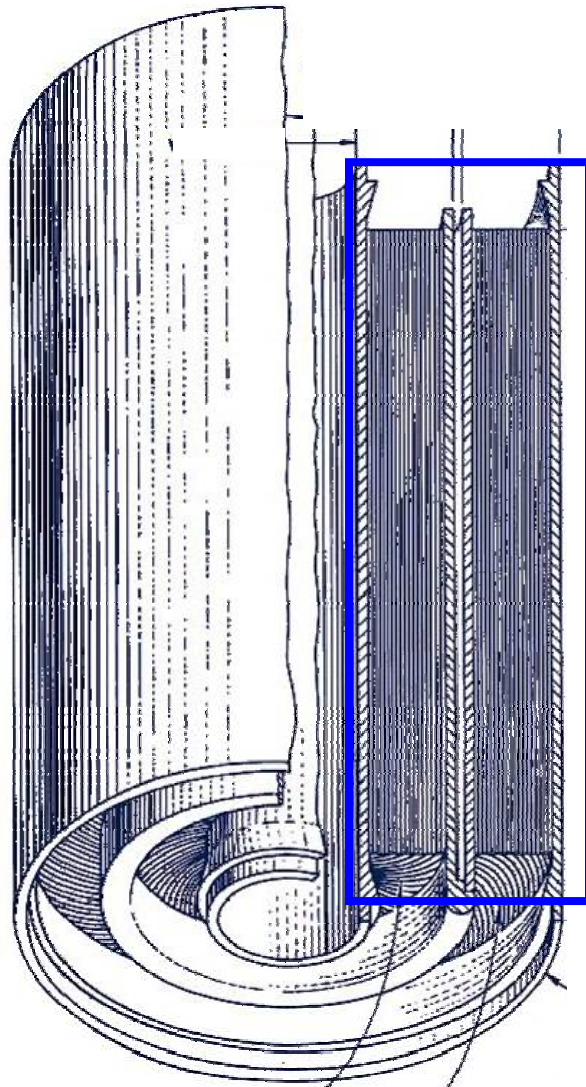


Fig. 2.10. Power contours in the Outer HFIR fuel elements (LEU at left, HEU at right) at BOL.



**Regions of core shown in
succeeding graphs**

Fig. 2.11. Sections of fuel elements visualized in succeeding graphs.

Burnup distribution in LEU core
 (maximum burnup fraction is 0.61)

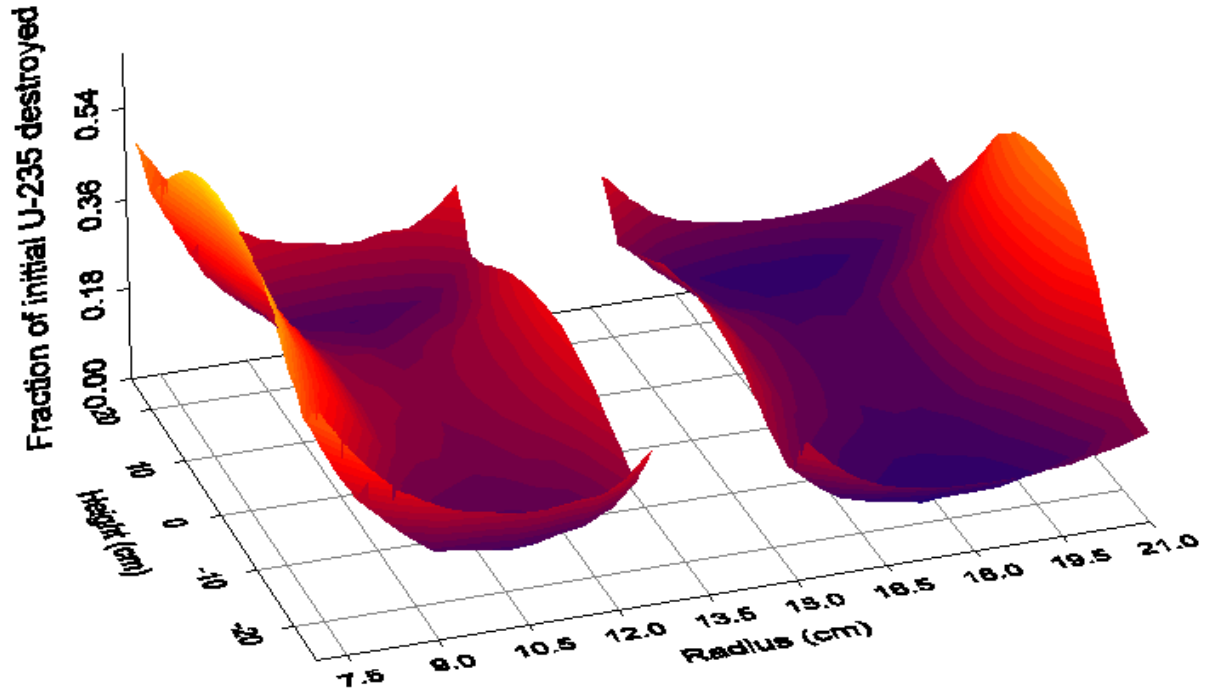
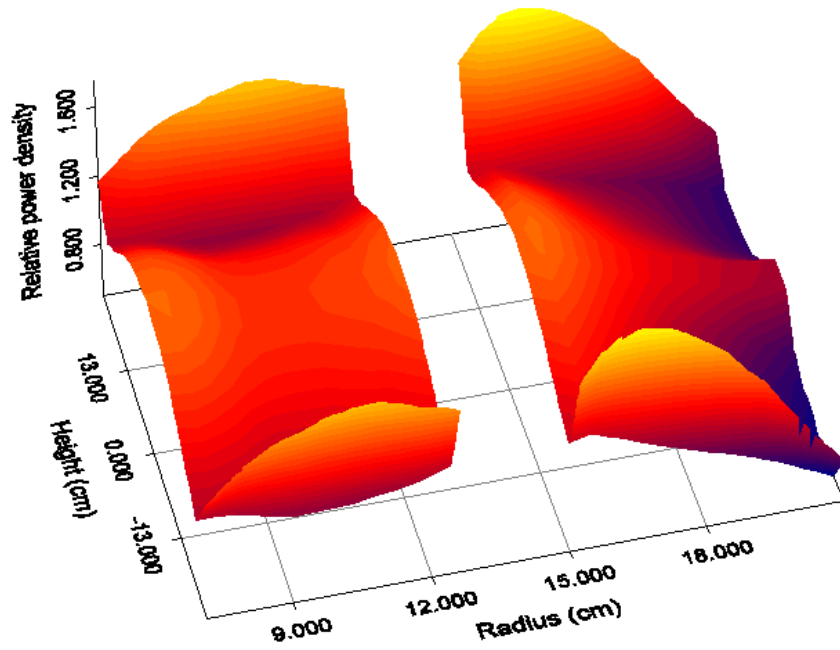


Fig. 2.12. Burn-up distribution in LEU core at EOL.

Table 2.4. Comparison of fuel meat thicknesses for LEU and HEU fuel plates

Distance along inner element plate (cm)	Thickness of fuel meat (mils)		Distance along outer element plate (cm)	Thickness of fuel meat (mils)	
	LEU	HEU		LEU	HEU
0.252	5.0	10.2	0.191	9.0	15.3
0.448	5.0	11.6	0.216	9.9	15.6
1.203	7.4	15.5	0.395	14.0	16.9
2.439	10.1	20.5	1.134	18.0	23.0
3.811	11.8	24.4	2.256	18.0	27.1
5.314	12.2	24.6	3.449	15.8	25.5
6.969	10.9	21.5	4.655	10.2	20.7
7.985	8.4	18.6	5.908	6.7	14.7
8.091	8.2	18.3	6.731	5.3	11.5

HEU core beginning of cycle power distribution



HEU core end of cycle power distribution

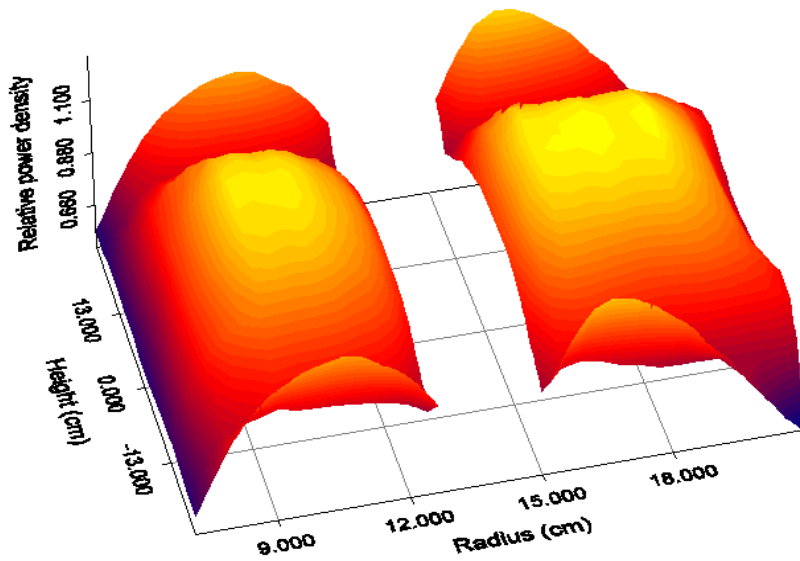
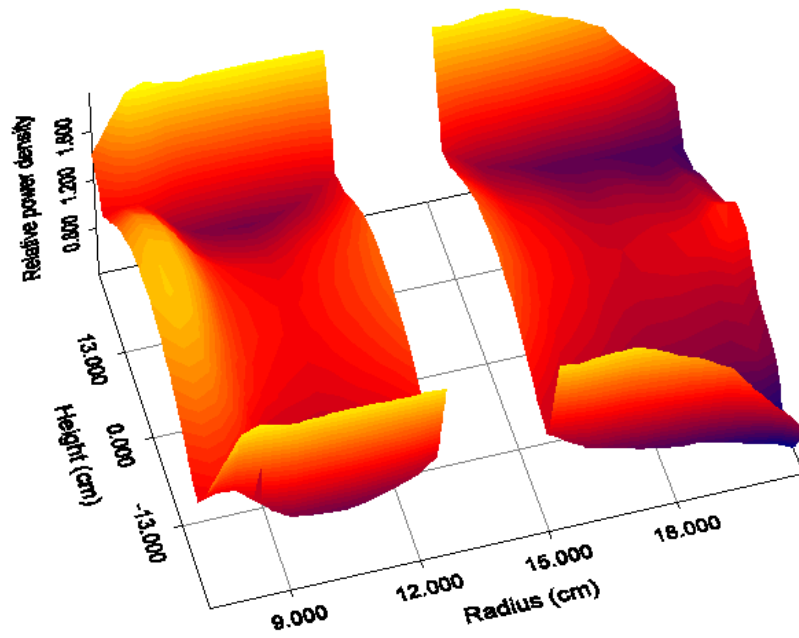


Fig. 2.13. Power distribution in HEU core at BOL and EOL.

LEU core beginning of cycle power distribution



LEU core end of cycle power distribution

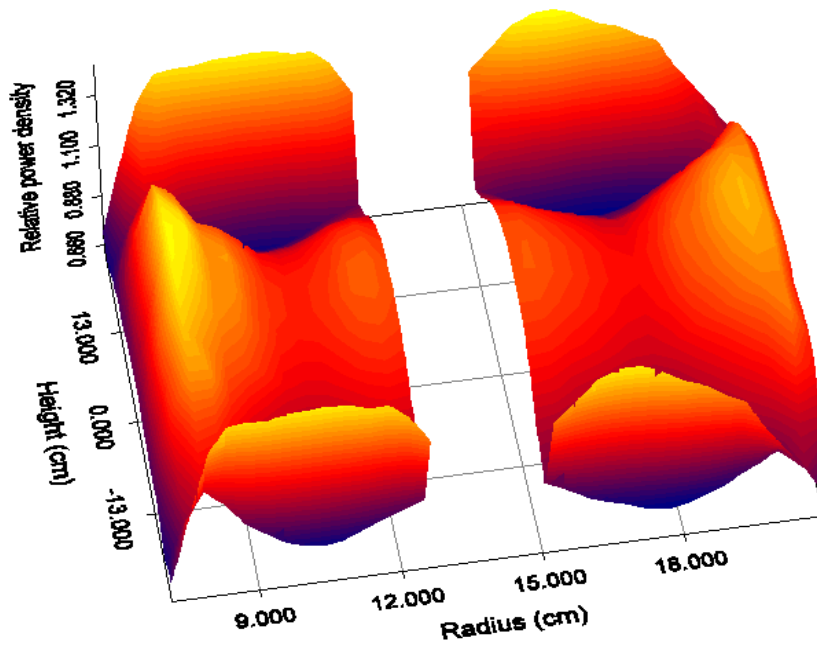


Fig. 2.14. Power distribution in LEU core at BOL and EOL.

As seen in Table 2.5, the peak thermal flux in the Be reflector in HFIR, with the graded LEU fuel, is reduced by approximately 12 percent compared to the reference HEU core calculations. This is consistent with the MCNP calculations for thermal flux reductions presented in Table 2.3, namely, the peak Be reflector thermal neutron flux is reduced by about 9 percent in the LEU case vs. the HEU case. In Table 2.6, it is seen that the peak thermal neutron flux in the central FTT region is not reduced significantly, and could in fact be slightly increased. The reference VENTURE case has a small amount of target material being irradiated which reduces the peak FTT thermal flux slightly. A subsequent further graded LEU fuel design has a slightly larger FTT peak thermal neutron flux level because the fuel mass was further reduced from the LEU (graded) case presented above.

In Table 2.6, major isotopics are presented for the LEU cases vs. the reference HEU case, as calculated with BOLD VENTURE. It is very apparent that the large concentration of ^{238}U in the LEU cores results in a buildup of approximately 260 g of ^{239}Pu in the HFIR core by EOL. At EOL, the LEU cores still contain approximately 16.5 kg of ^{235}U .

Further grading of the LEU core fuel is leading to a slightly-reduced ^{235}U content, as the grading process involves a minimization of the peak power density zones in the IFE and OFE. It is informative to mention that the peak power density, as calculated in VENTURE, in subsequent graded LEU cores has dropped to 2890 W/cm³, down from 3114 W/cm³ in the initial graded LEU case discussed in this interim report. By comparison, the VENTURE calculation of the reference HEU case has a peak power density of 2912 W/cm³.

Table 2.5. Peak thermal neutron flux levels as predicted by VENTURE for HEU and LEU cases

HFIR Core	Peak Thermal Neutron Flux in FTT Region	Peak Reflector Thermal Neutron Flux
HEU ref (no control abs)	2.4841E15	1.5308E15
LEU (No control absorbers)	2.7802E15	1.3594E15
LEU (graded, no control)	2.7946E15	1.3689E15
HEU ref (control absorbers)	2.5956E15	1.5613E15
LEU (Control absorbers)	3.0726E15	1.3658E15
LEU (graded, control abs)	3.0796E15	1.3754E15

Table 2.6. Comparison of HFIR isotope content (kg) in LEU and HEU cores, at BOL and EOL

Nuclide	HEU		LEU		LEU graded	
	BOL	EOL	BOL	EOL	BOL	EOL
^{235}U	9.46937	6.73844	19.3578	16.5737	19.2639	16.4795
^{239}Pu	9.0046e-6	1.2413e-2	0	0.26195	0	0.25852
^{238}U	0.55528	0.53420	78.3762	77.9726	77.1926	76.7934

3.0 THERMAL HYDRAULIC ANALYSES

Radial and axial mesh definitions and time-dependent power distributions from the neutronics calculations, along with assumptions on fuel manufacturing parameters and uncertainties (Ref. 1) were input to the HFIR steady state heat transfer code (HSSHTC, Ref. 1). Nominal and limiting operating conditions were determined with this software.

Operating power

The mechanics of the thermal-hydraulics analysis code are designed so that the heat transfer coefficient at any point in the iterative solution is calculated by using properties based on previous estimates for bulk water temperature and fuel plate surface temperature. The incipient boiling power level is also determined by iterative solution. The code calculates the incipient burnout power level by using coolant inlet pressure and temperature conditions. These calculations are performed by the code while automatically adjusting the reactor power until the surface heat flux predicted by the burnout correlation equals the hot spot heat flux. This condition occurs at only one “spot” on the entire fuel assembly out of all the mesh points in the calculation. The resultant power level, or incipient burnout power, is used in selecting the HFIR safety limit.

Because the LEU neutronics model contained additional radial zones not present in the HEU reference HFIR model, flux peaking factors – these account for increased local power densities due to fuel extending axially beyond the nominal manufacturing criteria – were needed for these added zones. The values assumed are provided in Table 3.1 and are similar in magnitude to those for the HEU core. When the final fuel grading is determined and manufacturing tolerances are known, these peaking factors will have to be recalculated.

Table 3.1. Flux peaking factors for fuel extending beyond normal axial boundaries of the fuel plate (flow entrance and exit)

<i>Zone in model</i>	<i>Inner element</i>	<i>Outer element</i>
1	1.00	1.00
2	1.00	1.00
3	1.00	1.00
4	1.23	1.23
5	1.25	1.23
6	1.41	1.26
7	1.44	1.35
8	1.44	1.35
9	1.44	1.35
10	1.43	1.31
11	1.30	1.23
12	1.20	1.00
13	1.00	1.00
14	1.00	1.00

The SCRAM setpoint for HFIR (from Ref. 2) operating power is 30 percent over nominal power. The limiting control setting for coolant pressure for HFIR is 100 pounds per square inch (psi) below nominal operating pressure (375 psia for the core inlet). Reactor operating power is determined by executing the HFIR steady state heat transfer code (HSSHTC) with a core inlet pressure of 375 psia,

determining incipient boiling power by the iterative solution described previously, and then dividing the incipient boiling power by 1.3.

The current operating power for HFIR with HEU fuel is 85 MW. The ratio of LEU incipient boiling power to HEU incipient boiling power as a function of time-in-fuel-cycle is shown in Table 3.2. Though incipient boiling power increases during the cycle (due to the burnout of high power density locations), the maximum allowable operating power for the reactor is kept constant during the cycle and is set equal to the minimum of all time steps. For both the current HEU cycle and the preliminary LEU design, this minimum occurs at beginning-of-life (though at 0.6 days, the HEU incipient boiling power has increased slightly more rapidly than that of the LEU cycle). The observation that the LEU incipient boiling power is less than the HEU value is due to higher peak power density in the LEU cycle relative to the HEU cycle.

Table 3.2. Incipient boiling power ratios

Time in fuel cycle (days)	Ratio of LEU incipient boiling power to HEU incipient boiling power
0.0	0.814
0.6	0.800
1.8	0.821
7.2	0.823
14.1	0.835
18.8	0.841
21.2	0.844
23.5	0.848
26 ^a	0.851

^a end of cycle at 27 days

For the preliminary LEU core, the limit on operating power due to the incipient boiling limit is found to be 69 MW, a 19 percent decrease from the current, HEU core. Fuel grading studies are continuing and are expected to reduce the incipient-boiling penalty for the LEU cycle by reducing local power peaking.

Conditions at incipient boiling limit locations

Results from the HSSHTC for various times in the fuel cycle are presented in Table 3.3. Corresponding data for the reference HEU fuel cycle are contained in Ref. 1 and reprinted below as Table 3.4

Incipient boiling powers in Table 3.3 have been adjusted by a bias identified by comparing calculated HEU power densities with experimentally measured values. For an LEU fuel, this bias would have to be confirmed by physics experiments with LEU fuel.

Impact of manufacturing tolerances/uncertainties on operating power

To estimate the impact of manufacturing uncertainties on the incipient boiling power limit, the HSSHTC input was modified to set all uncertainty factors to 1.0. The interpretation of this assumption is that all dimensions are precisely at their nominal values, there are no “cold” plates and no “hot” plates, no “sinusoidal longitudinal waves” due to “slumping” or no warping of fuel plates,

no radiation swelling, no fuel extending beyond the nominal end of the fuel plate, etc. Furthermore, the SCRAM setpoint is insignificantly higher than maximum operating power and the limiting control setting for system pressure at core inlet is insignificantly lower than 475 psia. For the LEU HFIR core, the incipient boiling power for this fictional, “nominal” case is 204 MW for BOL conditions and 266 MW for EOL conditions. The equivalent values for HEU are 276 MW at BOL and 316 MW at EOL. The magnitude of the differences between these values and the operating powers noted previously serves to emphasize the need for accuracy in all manufacturing uncertainties and the need to understand in-reactor phenomena such as instrument uncertainty and safety limits as well as fuel physical phenomena such as radiation swelling.

Table 3.3. LEU burn-up-dependent heat transfer data—incipient boiling criteria

Time into cycle	BOC	14.1 d	26.0 d
Limiting power level, MW (by ratio to HEU)	89.9	108.4	116.7
Limiting heat flux:			
Location, fuel element; across plate, along plate (cm)	Inner 0.448, 50.5	Inner 0.448, 50.5	Inner 0.448, 50.5
Thermal expansion of clad plus oxide thickness at limiting location (microns)	22	37	46
Heat flux, Btu/h-ft ²	3.07(10 ⁶)	2.83(10 ⁶)	2.85(10 ⁶)
Bulk water temperature, °F	259	276	277
Clad surface temperature, °F	423	422	422
Heat transfer coefficient, Btu/h-ft ² , °F	17,216	18,125	18,292
Flow rate, lb/s-in. width	0.7256	0.7095	0.6985
Pressure, psia	265	264	263
Maximum hot streak outlet bulk water temperature:			
Location, fuel element; across plate, (cm)	Inner, 0.488	Inner, 0.488	Inner, 0.488
Magnitude, °F	259	259	277
Flow rate, lb/s-in. width	0.7256	0.7095	0.6965
Minimum flow rate:			
Location, fuel element, cm	Inner, 5.3	Outer, 5.3	Outer, 5.3
Magnitude, lb/s-in. width	0.6819	0.6597	0.6335
Bulk water temperature at outlet, °F	234	253	274

Table 3.4. Burn-up-dependent heat transfer data—incipient boiling criteria – for HEU fuel

Time into cycle	BOC	1.014 d	11.57 d	22.72 d	25.0 d
Limiting power level, MW	110.63	120.89	116.51	116.34	120.35
Limiting heat flux:					
Location, fuel element (<i>i,j</i>)	Outer (3,29)	Inner (5,29)	Inner (5,29)	Inner (5,29)	Outer (4,29)
Heat flux, Btu/h-ft ²	2.80E+6	2.81E+6	2.79E+6	2.87E+6	2.70E+6
Bulk water temperature, °F	274	276	278	275	286
Surface temperature, °F	422	422	422	422	422
Heat transfer coefficient, Btu/h-ft ² , °F	18,920	19,250	19,375	19,525	19,850
Flow rate, lb/s-in. width	0.7473	0.6754	0.6468	0.6421	0.6684
Pressure, psia	264	264	264	263	263
Maximum hot streak outlet bulk water temperature:					
Location, fuel element (<i>i</i>)	Outer (4)				
Magnitude, °F	275	285	282	282	286
Flow rate, lb/s-in. width	0.7027	0.6948	0.6650	0.6594	0.6684
Minimum flow rate:					
Location, fuel element (<i>i</i>)	Inner (4)	Inner (5)	Inner (5)	Inner (5)	Inner (5)
Magnitude, lb/s-in. width	0.6848	0.6754	0.6468	0.6421	0.6530
Bulk water temperature at outlet, °F	271	276	278	275	273

^aReactor conditions based on 130°F coolant inlet temperature and 368-psig reactor pressure (equivalent to 375-psia fuel assembly inlet pressure). Coolant inlet temperature uncertainty factor U_6 is set to 1.0.. Locations (i,j) defined in Ref. 1

Results from the HSSHTC for various times in the fuel cycle are presented in Table 3.5. Note that there is no oxide growth on the aluminum clad during the fuel cycle in the results shown in Table 3.5. Results for the current, HEU fuel cycle are shown in Table 3.6. The heat flux at the hot spot does not increase from the Table 3.3 value by the same ratio as the incipient boiling powers because the fuel extension factors (Table 3.1) have been set to one in the case shown in Table 3.4 and the hot spot is at the base of the fuel plate.

Table 3.5. LEU burn-up-dependent heat transfer data – incipient boiling criteria - with perfectly engineered elements and perfect reactor operation

Time into cycle	BOC	14.1 d	26.0 d
Limiting power level, MW	204	246	266
Limiting heat flux:			
Location, fuel element; across plate, along plate (cm)	Inner, 0.448, 50.5	Inner, 0.448, 50.5	Inner, 0.448, 50.5
Thermal expansion of clad plus oxide thickness at limiting location (microns)	0	0	0
Heat flux, Btu/h-ft ²	4.05(10 ⁶)	3.69(10 ⁶)	3.71(10 ⁶)
Bulk water temperature, °F	279	296	295
Clad surface temperature, °F	451	450	451
Heat transfer coefficient, Btu/h-ft ² , °F	21,703	22,287	22,269
Flow rate, lb/s-in. width	1.1283	1.1278	1.1254
Pressure, psia	360	360	360
Maximum hot streak outlet bulk water temperature:			
Location, fuel element; across plate, (cm)	Inner, 0.448, 50.5	Inner, 0.448, 50.5	Inner, 0.448, 50.5
Magnitude, °F	279	296	296
Flow rate, lb/s-in. width	1.1283	1.1278	1.1254
Minimum flow rate:			
Location, fuel element, cm	Outer, 8.09	Outer, 2.439	Inner, 0.252
Magnitude, lb/s-in. width	1.1118	1.1167	1.1167
Bulk water temperature at outlet, °F	208	236	249

Table 3.6. Burn-up-dependent heat transfer data—incipient boiling criteria – with perfectly engineered elements and perfect reactor operation for HEU fuel

Time into cycle	BOC	11.57 d	25.0 d
Limiting power level, MW	276	315	316
Limiting heat flux:			
Location, fuel element; across plate, along plate (cm)	Outer, 0.191, 50.1	Outer, 0.191, 50.1	Outer, 0.627, 50.1
Thermal expansion of clad plus oxide thickness at limiting location (microns)	0	0	0
Heat flux, Btu/h-ft ²	3.60(10 ⁶)	3.41(10 ⁶)	3.48(10 ⁶)
Bulk water temperature, °F	299	308	305
Surface temperature, °F	450	450	450
Heat transfer coefficient, Btu/h-ft ² , °F	23,357	22,676	22,612
Flow rate, lb/s-in. width	1.1320	1.0997	1.0991
Pressure, psia	359	359	359
Maximum hot streak outlet bulk water temperature:			
Location, fuel element; distance across plate (cm)	Outer, 0.191	Outer, 0.191	Outer, 0.627
Magnitude, °F	299	308	305
Flow rate, lb/s-in. width	1.1320	1.0997	1.0991
Minimum flow rate:			
Location, fuel element; distance across plate (cm)	Outer, 6.6	Outer, 6.6	Inner, 0.234
Magnitude, lb/s-in. width	1.1157	1.0941	1.0907
Bulk water temperature at outlet, °F	229	266	236

4.0 PERFORMANCE INDICATORS

Availability Factor (cycle length and operating power)

Both the HEU fuel cycle and the LEU fuel cycle are calculated to achieve the same end-of-life burnup – 2295 MWD. The allowable operating power for the LEU cycle due to the incipient boiling limit would be less than the HEU cycle by 19 percent. Consequently, the resulting cycle length for the LEU fuel at the reduced power level would be 19 percent longer than the current cycle – 32 days instead of 27. Assuming that between-cycle time is independent of power level and cycle length, the availability of the reactor would increase with LEU, albeit at a lower operating power. Assuming the 19 percent power reduction, the margins-of-safety for the LEU fuel cycle are not less than the safety margins documented in the HFIR Updated Safety Analysis Report (Ref. 2). To regain the current

operating power level, a more detailed analysis is required of the assumed uncertainties. Such analysis is beyond the scope of current effort.

Flux in beryllium reflector

In Ref. 1, the reflector performance indicators are identified as being the flux of cold neutrons from the cold source, the thermal fluxes at the ends of HB-1, 2, and 3 beam tubes, and the thermal flux values at the neutron activation analysis sites. These indicators have not been calculated but the values of the thermal and fast fluxes at the peak thermal flux location in the beryllium reflector have been calculated for BOL and EOL conditions. A comparison of physics parameters for the current HEU cycle and LEU cycle is provided in Table 4.1.

Table 4.1. Reflector flux performance^a

Parameter ^a	HEU (current) fuel		LEU fuel				Change in performance %(LEU-HEU)/HEU			
	BOL	EOL	BOL		EOL		BOL		EOL	
			85 MW	69 MW	85 MW	69 MW	85 MW	69 MW	85 MW	69 MW
Peak thermal flux in reflector [10^{15} n/(cm ² s)]	0.920	1.54	1.00	0.81	1.39	1.13	8.7	12.0	-9.7	26.6
Fast/thermal flux ratio at thermal peak	0.260	0.229	0.096		0.092		-63.08		-59.83	
Radial location of peak (cm)	28.8	27.6	29.4		28.8		2.08		4.35	
Axial location of peak (cm)	-1.5	-1.5	-1.5		-1.5		0.00		0.00	
Volume of reflector with thermal flux > 80% of maximum (L)	40.5	44.9	49.6		56.1		22.47		24.94	
Inner radius of 80% of maximum thermal flux (cm)	24.1	24.1	24.1		24.1		0.00		0.00	
Outer radius of 80% of maximum thermal flux (cm)	36.1	35.0	36.8		36.4		1.94		4.00	
Upper axial location of 80% of maximum thermal flux (cm, at radial peak)	10.3	14.0	12.1		14.6		17.48		4.29	
Lower axial location of 80% of maximum thermal flux (cm, at radial peak)	-12.7	-14.2	-13.6		-14.7		7.09		3.52	

^a 0, 0 point is at the centerline of the inner element, at the axial mid-plane of the element

The LEU case provides a higher thermal flux at the peak location in the beryllium reflector at beginning-of-life than exists in the current HEU cycle if the comparison is made at the same power level for both cycles. However, the combination of the poorer thermal hydraulic performance of the LEU fuel and the differing patterns of burnup yield a 27 percent reduction in thermal flux in the reflector at end-of-cycle. The location of the thermal flux peak and volume corresponding to 80 percent of the peak thermal flux value are generally unchanged – an important observation because the beam tubes could not be relocated to new positions in the beryllium reflector without manufacturing a new reflector and pressure vessel.

Isotope Production and Materials Irradiation

While several material irradiation positions are located in the beryllium reflector, currently all irradiations and isotope production is performed in the central target region of the reactor. A comparison of physics parameters for the current HEU cycle and LEU cycle is provided in Table 4.2.

Table 4.2. Central target flux performance^a

Parameter ^a	HEU (current) fuel		LEU fuel				Change in performance %(LEU-HEU)/HEU			
	BOL	EOL	BOL		EOL		BOL		EOL	
			85 MW	69 MW	85 MW	69 MW	85 MW	69 MW	85 MW	69 MW
Peak thermal flux in reflector [10^{15} n/(cm ² s)]	2.586	2.608	3.15	2.56	2.86	2.32	21.8	-1.0	9.7	11.0
Fast/thermal flux ratio at thermal peak	0.412	0.390	0.149		0.149		-63.83		-61.79	
Radial location of peak (cm)	0.4	0.4	0.4		0.4		0.00		0.00	
Axial location of peak (cm)	1.5	-1.5	1.5		-1.5		0.00		0.00	
Volume of reflector with thermal flux > 80% of maximum (L)	1.2	1.3	1.8		1.7		50.00		30.77	
Inner radius of 80% of maximum thermal flux (cm)	0	0	0		0		-		-	
Outer radius of 80% of maximum thermal flux (cm)	4.2	4.6	4.6		4.8		9.52		4.35	
Upper axial location of 80% of maximum thermal flux (cm, at radial peak)	15.9	14.6	15.5		14.5		-2.52		-0.68	
Lower axial location of 80% of maximum thermal flux (cm, at radial peak)	-15.5	-14.7	-15.1		-14.6		-2.58		-0.68	

^a 0, 0 point is at the centerline of the inner element, at the axial mid-plane of the element

For equivalent power levels, the peak thermal flux in the target region for the LEU cycle exceeds that of the current cycle throughout the cycle. This characteristic could be desirable for materials irradiation. However, the significant drop in fast (and presumably epithermal) flux and rise in thermal flux could hinder californium production. The reduction in operating power for the LEU cycle results in a net reduction in the thermal flux in the target region though the level of reduction is considerably less than in the reflector region.

Plutonium production

As noted in Section 2.0, plutonium production in the LEU cycle is a factor of 20 greater than the current HEU fuel cycle. The current planning schedule for HFIR is to have eight fuel cycles per year. Annual plutonium production at HFIR with an LEU fuel cycle would be two kilograms.

5.0 IMPLICATIONS FOR FUEL PLATE DESIGN AND FABRICATION

Caution should be exercised in regard to directing fuel plate design based on the preliminary studies documented here. However, five points are apparent from work completed to date.

- 1) The fuel thickness in the inner element does not vary significantly as a function of distance along the plate. Thus the presence of boron in the filler region of the plate does not impact the power distribution because there is no spatial variability in the boron distribution. The boron does seem to act to shift the power from the inner to the outer element but it is not clear whether the effect could be achieved via other design options.
- 2) The axial power peaks, especially at the base of the fuel plate (coolant exit) are driving factors in limiting the operating power for the LEU cycle. Since the ^{235}U loading in the LEU core must be twice the value of the HEU core, the LEU core can never achieve lower local power densities than the HEU core regardless of the effort spent in grading the fuel (but it can be minimized). This conclusion results from the observation that the neutronic hot spot is at the lower fueled edge of the core. The average ^{235}U density along the lower edge will always be twice the value of the HEU core. However the flux in that region will be relatively insensitive to the ^{235}U content because it will always be well thermalized due to the presence of water below the fuelled region of the core. These two factors mandate that the local power density somewhere along the lower edge of the LEU core will always be higher than the maximum local power density along the lower edge of the HEU core. While it is outside the scope of the current study, future work could consider a modification to the plate design. This modification could take the form of grading the fuel in the axial direction as well as the radial direction – a task difficult to envision for particle fuels. Metal fuel production procedures, perhaps, could accommodate two dimensional grading. Another possible solution could be achieved by modifying the fuel plate to include a neutron-absorbing zone below the lower edge of the fuel in order to reduce the axial peak. It is not known if a two-axial-zone fuel plate could be produced with the current powder-based fabrication process.
- 3) The minimum fuel thickness is 0.0127 cm (5 mils) with a reported manufacturing uncertainty of 1 mil. This results in a 20 percent uncertainty in the fuel distribution which exceeds the currently assumed value in these calculations (per Ref. 1) of 12%. Maintaining the current HFIR criterion of 12 percent would mean that the uncertainty in the U-10Mo thickness would have to be 0.6 mils.
- 4) If further studies of fuel grading and the judicious use of burnable poison are not successful in eliminating the power peaking issue, then the impact of these higher power peaking factors in the LEU cycle relative to the HEU cycle could be mitigated by reducing the uncertainty factors that are applied in the thermal hydraulic analysis. Consequently, a rigorous investigation of the uncertainty factors and determination of appropriate values to be applied to an LEU fuel would be the logical study to follow the current analyses.
- 5) Since the thickness of the fuel meat region in the LEU plates is considerably less than that of the current HEU plates, it could be possible to reduce the thickness of the HFIR fuel plate from the current value of 50 mils to 40 mils, increase the number of fuel plates in the inner and outer elements, thereby increasing the fuel loading and increasing the cycle length. The heat transfer surface area would be increased so for a fixed power level, the heat flux would decline. The water-to- ^{235}U ratio would be unchanged. Only aluminum would be removed from the core. Hence the critical mass should remain generally unchanged. Such a design is beyond the scope of the current study.

6.0 REFERENCES

- 1) R. T. Primm III, R. J. Ellis, J. C. Gehin, D. L. Moses, and J. L. Binder, *Assumptions and Criteria for Performing a Feasibility Study of the Conversion of the High Flux Isotope Reactor Core to Use Low-Enriched Uranium Fuel*, ORNL/TM-2005/269, February 2006.
- 2) ORNL/HFIR/USAR/2344, HFIR Updated Safety Analysis Report, Revision 5, May 2005.

Appendix

FUEL PARAMETER LIST

The key parameters related to fuel behavior are temperature, fission rate, and fission density of the fuel as a function of time. RERTR program fuel development and qualification testing must cover fuel operating requirements in high-power reactors. While the emphasis of testing is on encompassing limiting conditions, it is also helpful to know the values of these parameters under nominal conditions. Since the main parameters that are required are not the ones usually tabulated for reactor operations, the list below requests more common parameters from which fuel testing conditions can be derived. Data provided are for current fuel and currently licensed operating conditions (HEU, U_3O_8 in aluminum).

Fuel Parameter	Value
Nominal Conditions	
1. U-235 content of fresh fuel element	9.4 kg
2. Enrichment of fresh fuel	93%
3. Fuel type and uranium density in fuel meat	U ₃ O ₈ in aluminum, see ORNL/TM-2005/269, Fig. 3.1
4. Nominal fuel meat thickness	0.0508 cm (20 mils)
5. Nominal cladding thickness (cm)	0.0254
6. Nominal water channel width (cm)	0.127
7. Element average and peak discharge burnup, % U-235	0.28 (average); 0.72 (peak)
8. Average number of full-power days to discharge	27
9. Peak plate power density at beginning of life (with and without hot channel factors)	1.7 (calculated), 1.6 (measured) Hot channel factors are irrelevant; however, fuel fabrication tolerances are relevant and are position dependent. See ORNL/TM-2000/309, Appendix A9
10. Specify breakdown of hot channel factors included in item 9.	See ORNL/TM-2005/269, Table 4.1
11. Average nominal plate power density in the plate with peak power density at beginning of life	Approximately 2000 watts/cm ³ Inner element
12. Peak plate power density at end of life (with and without hot channel factors)	1.16 (no factors) 1.51 (end fuel deviation)
13. Average nominal plate power density in the plate with peak power density at end of life	Approximately 2000 watts/cm ³ Outer element
14. Peak fuel meat centerline temperature or surface heat flux at beginning of life (with and without hot channel factors)	See ORNL/TM-2005/269, Table 2.5
15. Specify breakdown of hot channel factors included in item 14, if different from those in item 10.	Same as for part 10
16. Average nominal fuel meat centerline temperature or surface heat flux in the plate with peak centerline temperature or surface heat flux at beginning of life	163°C (nominal meat)
17. Peak fuel meat centerline temperature or surface heat flux at end of life (with and without hot channel factors)	Approximately 285 °C (the peak value usually occurs in the hot channel)
18. Average nominal fuel meat centerline temperature or surface heat flux in plate with peak centerline temperature or surface heat flux at end of life	163°C (nominal meat)
19. Hot spot conditions (assumed size, location, movement)	See ORNL/TM-2005/269, Tables 2.2 and 2.3

Limiting Conditions	
20. Maximum allowable surface heat flux	Variable, determined by calculating time dependent burnout heat flux at core inlet pressure of 375 psia and dividing that power by 1.3
21. Maximum allowable power density	Variable, determined by calculating time dependent burnout heat flux at core inlet pressure of 375 psia and dividing that power by 1.3
22. Maximum allowable U-235 burnup (specify peak or average)	No limit
23. Maximum allowable plate swelling	Variable, determined by calculating time dependent burnout heat flux at core inlet pressure of 375 psia and dividing that power by 1.3
24. Minimum water channel width	0.1016 cm (40 mils) at BOL
25. Other limiting conditions related to power, burnup, or	Spent fuel shipping cask license limits burn-up

temperature	to 2300 MWD.
Fuel Specification	
26. U-235 homogeneity specification at plate center and dog bone regions	See ORNL/TM-2005/269, Table 2.5 and ORNL/TM-2000/309, Appendix A9
27. Allowed local variation from nominal loading and spot size over which it occurs	+27% over area of 0.026 cm ² +12%/-12% over area of ~2.5 cm ²
28. Fuel meat porosity limits (upper and lower bounds)	This limit not used. Surface area of U ₃ O ₈ particles is measured. Surface area shall be less than 0.05 m ² /g
29. Size of maximum debond region over fuel meat (cm ²)	0.026
Additional Requirements or Comments	

INTERNAL DISTRIBUTION

- | | | | |
|------|------------------|--------|------------------------------|
| 1. | J. L. Binder | 9. | Central Research Library |
| 2-3. | R. J. Ellis | 10. | ORNL Laboratory Records-RC |
| 4-5. | J. C. Gehin | 11-12. | ORNL Laboratory Records-OSTI |
| 6. | D. L. Moses | 13. | RRD-DCC |
| 7-8. | R. T. Primm, III | | |

EXTERNAL DISTRIBUTION